Homology-directed repair involves multiple strand invasion cycles in fission yeast

Amanda J. Vines, Kenneth Cox, Bryan A. Leland, and Megan C. King*
Department of Cell Biology, Yale School of Medicine, New Haven, CT 06520

ABSTRACT Homology-directed repair of DNA double-strand breaks (DSBs) represents a highly faithful pathway. Non–crossover repair dominates in mitotically growing cells, likely through a preference for synthesis-dependent strand annealing (SDSA). How homology-directed repair mechanism choice is orchestrated in time and space is not well understood. Here, we develop a microscopy-based assay in living fission yeast to determine the dynamics and kinetics of an engineered, site-specific interhomologue repair event. We observe highly efficient homology search and homology-directed repair in this system. Surprisingly, the initial distance between the DSB and the donor sequence does not correlate with the duration of repair. Instead, we observe that repair often involves multiple site-specific and Rad51-dependent colocalization events between the DSB and donor sequence. Upon loss of the RecQ helicase Rqh1 (BLM in humans) we observe rapid repair possibly involving a single strand invasion event, suggesting that multiple strand invasion cycles antagonized by Rqh1 could reflect ongoing SDSA. However, failure to colocalize with the donor sequence and execute repair is also more likely in *rqh1Δ* cells, possibly reflecting erroneous strand invasion. This work has implications for the molecular etiology of Bloom syndrome, caused by mutations in BLM and characterized by aberrant sister chromatid crossovers and inefficient repair.

INTRODUCTION

Homology-directed repair (HDR) is a conserved, high-fidelity mechanism for repairing DNA double-strand breaks (DSBs). Following recognition of the DSB by the MRN complex and 5′ to 3′ exonuclease-dependent end resection, faithful repair by HDR requires a Rad51-dependent homology search by the resultant nucleoprotein filament to locate a homologous donor sequence to use as a template. The sister chromatid available after replication is the most common template for repair (San Filippo *et al.*, 2008; Mimitou and Symington, 2009). In this case, the template is identical to the original sequence and homology search is likely to be temporally and nal sequence and homology search is likely to be temporally and spatially efficient due to sister chromatid cohesion (Seeber *et al.*, 2016; Haber, 2018). The homologous chromosome or an ectopic sequence can also be used as templates for repair, involving a more demanding homology search (Pâques and Haber, 1999; Mehta and Haber, 2014), but use of these templates can lead to loss of heterozygosity or genome instability (Renkawitz *et al.*, 2014). Therefore, high-fidelity repair hinges on the accurate choice of a homologous donor.

A successful long-range homology search (i.e., with a non–sister chromatid donor) requires that 1) the distant DSB and donor loci are able to encounter one another within the nucleus; 2) the Rad51-bound nucleoprotein filament can drive strand invasion of potential donors (leading to formation of a displacement [D-] loop); and 3) the homologous sequence is used as the template for new synthesis. Chromatin mobility likely facilitates the encounter rate and has been observed to increase upon DSB induction both locally at the DSB and globally (Miné-Hattab and Rothstein, 2012; Seeber *et al.*, 2013). The degree of induced mobility may be influenced by the type of damage induction (irradiation, DNA-damaging drugs such as zeocin, or site-specific nuclease induction), cell ploidy (chromatin density), the number of DSBs and whether a DSB has persisted long enough to activate checkpoint arrest (Miné-Hattab *et al.*, 2017; Zimmer and Fabre, 2019). Indeed, chromatin mobility can be induced by activation of the checkpoint response in the absence of

damage (Bonilla *et al.*, 2008). Notably, an initial decrease in mobility within the first hour following DSB induction has been observed in budding yeast with a single DSB (Saad *et al.*, 2014). This initial decrease in mobility may contribute to repair using "local" donor sequences such as the sister chromatid, while increased local and global mobility following cell cycle arrest may facilitate interactions with alternative sequences that are less desirable templates but allow for DSB repair.

The outcome of homology search is also impacted by the regulation of strand invasion by the nucleoprotein filament as it samples potential templates. Factors such as the BLM helicase (Rqh1 in *Schizosaccharomyces pombe*) are thought to dissolve D-loops, thereby driving non–crossover repair events (Lorenz *et al.*, 2014). Rqh1 likely promotes non–crossover products by favoring synthesis-dependent strand annealing (SDSA), in which strand invasion leads to new synthesis followed by dissolution of the D-loop, strand annealing that spans the initial DSB site, and repair (Symington *et al.*, 2014; Symington, 2016). However, to the best of our knowledge, direct observation of this Rqh1 activity has not yet been possible in vivo.

Here, we describe the development of a microscopy-based assay in diploid fission yeast to determine the dynamics and kinetics of an engineered, interhomologue repair event. Although the initial distance between DSB and donor sequence predicts the time to their first physical encounter, it fails to predict the time to repair**.** Instead, repair efficiency tends to correlate with the number of strand invasion events, with many repair events requiring multiple strand invasion cycles. In the absence of Rqh1, successful repair appears to require a single strand invasion event in a subset of cells, suggesting that multiple strand invasion cycles could reflect ongoing SDSA. This work therefore reveals the spatial and temporal events that influence homology-directed repair outcomes in living fission yeast cells.

RESULTS AND DISCUSSION
Microscopy assay to study interhomologue repair in living fission yeast
To monitor the timing and dynamics of homology search, we took advantage of a mating type mutant of *S. pombe* (*mat2-102*; Egel, 1973; Bodi *et al.*, 1991) to generate stable diploids. In all cases, one of the haploid strains contains a site-specific HO endonuclease cut site adjacent to the *mmf1* gene on chromosome II (Chr II), expresses Rad52(Rad22)-mCherry, and has a floxed marker at the *urg1* gene that facilitates efficient Cre-mediated integration of the HO endonuclease such that it is regulated by the uracil-regulated *urg1* promoter (Watson *et al.*, 2011). The other haploid strain has a 10.3 kb array of *lacO* repeats integrated adjacent to *mmf1* and expresses LacI-GFP (Figure 1A). Cells therefore have a single GFP focus and a diffuse distribution of Rad52-mCherry in the absence of HO endonuclease expression when visualized by fluorescence microscopy (Leland *et al.*, 2018) (Figure 1A). We have shown previously in haploid cells that such a system induces a site-specific and irreparable DSB during S-phase on both replicated copies upon addition of uracil to the growth media (Leland *et al.*, 2018). In this diploid system, the induced DSB can undergo interhomologue repair (Figure 1B), with the DSB searching the nuclear volume and utilizing the homology near *mmf1* on the *lacO* array-containing homologous chromosome as the donor sequence (Figure 1A). As we observed previously in haploid cells (Leland *et al.*, 2018), DSB induction and end resection lead to the recruitment of Rad52-mCherry, a proxy for the formation of the nucleoprotein filament that facilitates homology search and strand invasion, in ~15% of cells, which are typically

in S-phase (Supplemental Figure S1A). A number of factors likely contribute to this consistently low induction rate, including 1) the short time window of observation relative to bulk, end point repair assays; 2) prior leaky HO expression; and/or 3) potential interference with HO recognition site cleavage by stable nucleosomes, as in native HO mating type locus regulation in budding yeast (Laurenson and Rine, 1992; Haber, 1998). All cells in our system display transient and dim Rad52-mCherry foci during S-phase, likely due to endogenous replication stress (Supplemental Figure S1B). We occasionally observe long-lived Rad52 foci in a small subpopulation of cells (Supplemental Figure S1B)—this is in line with previous publications in a variety of contexts (Coulon *et al.*, 2006; Lorenz *et al.*, 2009; Sanchez *et al.*, 2012; Schonbrun *et al.*, 2013).

On the basis of these observations, we hypothesized that the formation of a Rad52-mCherry focus at the site-specific DSB could be inferred by progressive and long-lived (>15 min) Rad52 loading induced at S-phase. Indeed, cells without the induction of HO nuclease demonstrate only sporadic Rad52-mCherry loading (Supplemental Figure S1B). The percent of frames (taken every 5 min) in which a Rad52-mCherry focus is observed is significantly higher for cells with HO nuclease induction than without (Supplemental Figure S1C). This interpretation was further validated experimentally (see below).

An example of the time course of repair timing and chromatin dynamics within the three-dimensional nuclear context is presented in Figure 1C. Images were acquired at 5 min intervals for 3 h after addition of uracil to induce expression of the HO endonuclease. The LacI-GFP marking the donor sequence can be monitored throughout the movie. In this example, persistent Rad52-mCherry loading occurs at 40 min following nuclear division and persists up to 100 min following nuclear division (65 min total). Colocalization between the Rad52-mCherry–loaded DSB and the donor sequence first occurs at 90 min post–nuclear division and is observed again at 100 min post–nuclear division, with Rad52 eviction occurring 5 min later (105 min post–nuclear division). The relationship between loss of a persistent Rad52-mCherry focus and repair was affirmed by monitoring subsequent cell division (see example, Supplemental Figure S1D).

As this system relies on inferring on-target, site-specific DSBs, we next carried out several controls to rigorously test whether the range of dynamics we observe (see additional examples in Supplemental Figure S2, A–C) indeed reflect homology-directed repair and can be meaningfully interpreted. First, we determined the likelihood that the two *mmf1* loci would, at the diffraction limit of the light microscope, be found colocalized due to random fluctuations of the chromosomes in the absence of DSB induction. To this end, we generated a diploid strain in which a *lacO* array was integrated at both copies of *mmf1* (Figure 2, A and B) and assessed the frequency at which the two *lacO* foci were found to be coincident. Under our imaging conditions, we find that the two *lacO*-LacI-GFP foci cannot be resolved in ~10% of frames during G2 (the cell cycle stage when we monitor repair [Leland *et al.*, 2018], the majority of the *S. pombe* cell cycle) (Figure 2C). This is in stark contrast to the analysis of an aggregated cohort of wild-type (WT) cells containing only one *lacO* array (as in Figure 1A) with DSBs ($n = 21$), in which Rad52-mCherry foci colocalized with the LacI-GFP–tagged donor sequence in ~35% of 5 min frames (Figure 2C). Thus, the majority of colocalization events between the Rad52-mCherry–loaded DSB and the donor sequence require the presence of the DSB.

To further test whether the observed colocalization events require strand invasion, we examined cells lacking Rad51, which is required for all homology search and strand invasion during HDR.
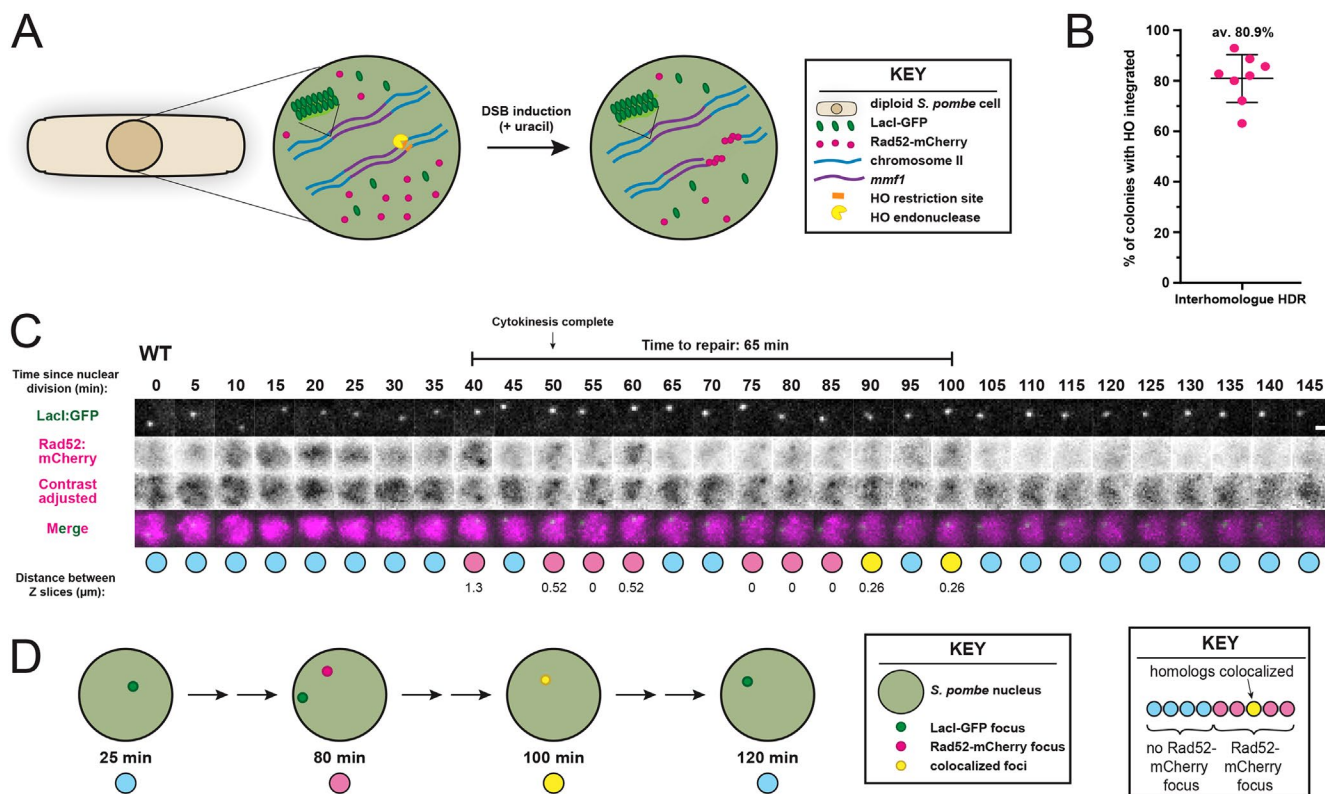
FIGURE 1: Fission yeast model system to monitor homology search during interhomologue repair in single, living cells. (A) Experimental design for the repair of a site-specific DSB in diploid fission yeast. A recognition site for the HO endonuclease is integrated adjacent to the *mmf1* gene on one copy of Chr II. On the other copy of Chr II there is a *lac* operator array integrated ~5 kb from *mmf1*. The other assay components include constitutive expression of LacI-GFP and Rad52-mCherry with inducible expression of the HO endonuclease from the uracil-regulated *urg1* promoter. (B) Interhomologue repair (mitotic recombination) is the dominant mode of homology-directed repair in diploid fission yeast. The proportion of cells expressing the HO endonuclease that undergo interhomologue repair, as determined by HO recognition site marker loss assay (see *Materials and Methods*). Data from eight biological replicates each containing between 50 and 200 colonies. Plot reflects mean and SD. (C) Efficient homology search and subsequent repair during interhomologue repair in fission yeast. Representative cell undergoing repair of the HO-induced DSB (see Supplemental Figure S2 for additional representative cells). Below the image series the events are indicated as blue circles (no Rad52-mCherry focus), pink circles (Rad52-mCherry focus present but not colocalized with the donor), or yellow circles (Rad52-mCherry focus present and colocalized with the donor) (see *Materials and Methods* for details). Contrast of Rad52-mCherry signal adjusted according to the full histogram of intensities where indicated. Scale bar = 1 µm. (D) Cartoon depicting examples of the key events during repair corresponding with the images in C: at 25 min, LacI-GFP is present at the donor before resection is evident; at 80 min, Rad52-mCherry is loaded at the DSB; at 100 min, there is colocalization of the Rad52-mCherry and LacI-GFP foci; and at 120 min, Rad52-mCherry is absent from the DSB.

Colocalization events between the induced DSB and donor sequence were strongly attenuated in *rad51Δ* cells (Figure 2, C and D), nearly to the level observed in the absence of damage in the control two *lacO* cells (Figure 2C) despite persistent Rad52-mCherry loading. This suggests that most encounters between the DSB and donor sequence are mediated by Rad51. We also analyzed the lifetime of DSB-donor sequence colocalization events in individual cells in all three conditions (Figure 2E). We observe that colocalization events in control two *lacO* cells without DNA damage and *rad51Δ* cells with DSB induction are short-lived compared with a broad distribution of lifetimes in WT cells, a conclusion reinforced by the difference in cumulative probability of colocalization frequency (Figure 2F).

A site-specific DSB promotes multiple encounters with the homologous donor

The characteristic time required to successfully orchestrate HDR in fission yeast remains to be fully defined. Near-complete recov-

ery of a site-specific I-PpoI–induced DSB at a "generic" locus or at the ribosomal DNA repeats in fission yeast took place within 4 h as measured by quantitative PCR (Ohle *et al.*, 2016), but events on the minutes timescale in single cells are lacking. Other assay systems often employ donor sequences with only short-range homology to the DSB or utilize a minichromosome. By contrast, here we monitor repair between true homologous chromosomes. In addition, we specifically monitor diploid cells during the time from the onset of long-range DSB end resection by accumulation of Rad52 (visualizable ~40–60 min following addition of uracil [see *Materials and Methods*] and with ~125 resected base pairs; Leland *et al.*, 2018) to the eviction of Rad52, which corresponds more closely to the period of HDR. Defined in this manner, we find that HDR is highly efficient. The mean time between Rad52-mCherry loading and eviction is ~50 min, although there is substantial cell-to-cell variation with an SD of ~20 min (Figure 3A).
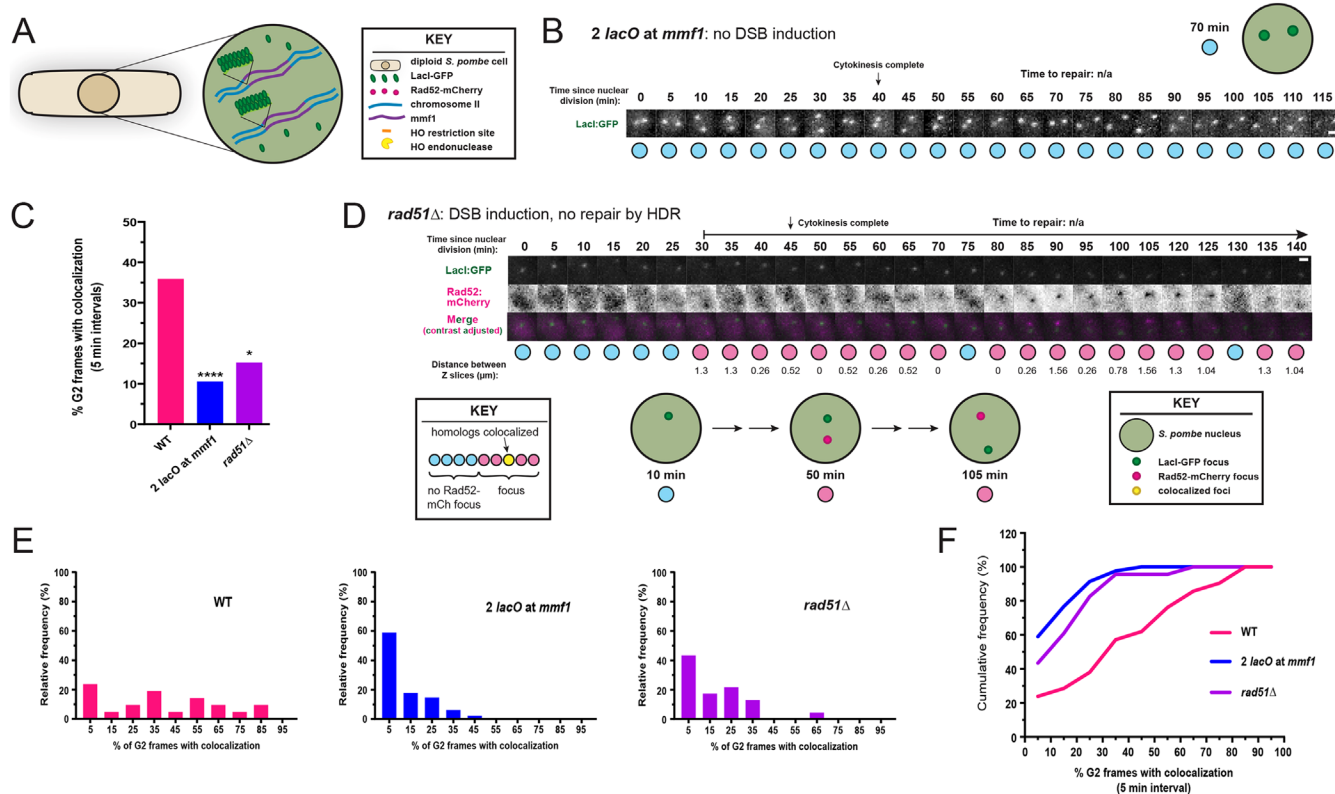
FIGURE 2: Colocalization of the DSB and donor sequence is driven by DSB formation and is Rad51-dependent. (A) Experimental design for monitoring of *mmf1* at both homologous Chr II loci in the absence of DSB induction (2 *lacO* at *mmf1* background). On both copies of Chr II there is a *lac* operator array integrated ~5 kb from *mmf1* (see *Materials and Methods*), and LacI-GFP is expressed to visualize both homologues. There is no DSB present. (B) Chr II homologues near the *mmf1* gene undergo minimal colocalization in the absence of an induced DSB. Z stack images of a nucleus from a representative 2 *lacO* at *mmf1* cell (see *Materials and Methods*). Imaged as described in *Materials and Methods*, with 5 min between each time frame (columns) and labeled relative to nuclear division. Scale bar = 1 μm. Top right: cartoon depicts an example of the key condition over the time course. LacI-GFP is present at both copies of *mmf1*. At 70 min there is no colocalization between these two sequences (as is true at other time points). (C) Colocalization of homologues near *mmf1* is largely dependent on DSB induction and Rad51. Frames in which cells were in G2 phase were analyzed for colocalization of the DSB and donor (for WT and *rad51Δ*, only cells judged to have persistent, site-specific DSBs [see *Materials and Methods*] were included) and averaged as a total percentage across all cells. Colocalization is that of the DSB (Rad52-mCherry) and donor sequence (LacI-GFP bound to *lacO* repeats at *mmf1*) (WT and *rad51Δ*) or both Chr II homologues in the absence of damage (2 *lacO* at *mmf1*). *$p < 0.05$, ****$p < 0.0001$, Kolmogorov–Smirnov test of cumulative distributions (of percentages from individual cells). WT: $n = 26$, 2 *lacO* at *mmf1*: $n = 129$, *rad51Δ*: $n = 23$. (D) The DSB induced by HO endonuclease is persistent in *rad51Δ* cells. Z stack images of a representative *rad51Δ*-induced cell imaged with 5 min between each time frame (columns) and labeled relative to nuclear division as described in *Materials and Methods*. Scale bar = 1 μm. Bottom, cartoon depicts examples of the key events over the time course: at 10 min, LacI-GFP is present at the donor; at 50 min, Rad52-mCherry is loaded at the DSB; and at 105 min, Rad52-mCherry persists at the DSB without having colocalized with the donor. (E, F) Colocalization between the DSB and donor sequence is far more prevalent in WT cells than in *rad51Δ* cells or for cells with two *lacO* arrays at *mmf1* in the absence of damage. (E) Relative frequency histograms of percentages of G2 frames with colocalization in individual 2 *lacO* at *mmf1* control cells ($n = 129$), *rad51Δ* DSB cells ($n = 23$), and WT DSB cells ($n = 21$) (≥5 G2 frames per cell). Colocalization is for the DSB (Rad52-mCherry) and donor sequence (LacI-GFP bound to *lacO* repeats at *mmf1*) (WT and *rad51Δ*) or both Chr II homologues in the absence of damage (2 *lacO* at *mmf1*). (F) Cumulative frequency histograms of data in E.

Our initial expectation was that repair time corresponds to a single homology search event culminating in strand invasion of the donor sequence by the DSB, new synthesis, and ultimate repair. In this case, we would expect that 1) the time to the first DSB-donor encounter and the time to repair are correlated, if not equivalent, and 2) the initial distance between the loci and the time to repair are correlated (Lee *et al.*, 2016). However, in this system we observed that the time to the first encounter and the time to repair are not correlated (Figure 3B). Additionally, we found that the initial distance

between the DSB and donor sequence does not correlate with repair time (Figure 3C), suggesting that an encounter per se is not the rate-limiting factor in HDR. Instead, we frequently observe multiple colocalization events in individual cells over the course of DSB repair (Figure 3D)—an example of such a cell is shown in Figure 3E. We therefore examined whether the initial distance between the DSB and donor sequence correlates with the time to the initial colocalization event. Indeed, our analysis confirmed such a relationship (Figure 3F). Given that most colocalization events are Rad51-dependent

(Figure 2, D–F), we infer that many cells undergo multiple strand invasion events between the DSB and donor sequence before the completion of repair. If true, we would expect repair time to be tied to the number of strand invasion events. Indeed, we observe a positive correlation, supporting this interpretation (Figure 3G). Given that multiple DSB-donor encounters are likely to be meaningful in HDR, we were concerned that we could underestimate the number of colocalization events given our observation window (5 min time points for several hours—see *Materials and Methods*), which was optimized to observe the entire repair process. When imaging WT cells with a site-specific DSB at 2 min intervals (2.5 times more frequently), we do observe a shift (of at most ~1 encounter per 30 min observation window) toward more colocalization events with the donor sequence (Supplemental Figure S3, A and B). However, more frequent sampling also leads to an increase in random encounters as revealed by analysis of the two *lacO* control strain (Supplemental Figure S3, A and B). Thus, while we may underrecord the number of colocalization events in some cases, we chose to utilize 5 min time points to maximize the likelihood of visualizing colocalizations that reflect meaningful strand invasion.

Cells lacking Rqh1 display a bimodal repair phenotype and likely require fewer homologous encounters for repair

On the basis of the prevalence of multiple encounters between the DSB and donor sequence and variability in repair timing, we next considered whether these kinetics reflect anti–recombination pathways that enforce HDR fidelity and/or non–crossover repair by SDSA. To address this, we tested the impact of deleting the *S. pombe* RecQ helicase, Rqh1, orthologous to human BLM. Rqh1 is established to dissolve D-loops (van Brabant *et al.*, 2000; Bachrati *et al.*, 2006; Hope *et al.*, 2007) and also contributes to DSB end resection in some contexts (Nanbu *et al.*, 2015; Yan *et al.*, 2019). However, we previously demonstrated that Rqh1 is dispensable for end resection in otherwise WT fission yeast cells (Leland *et al.*, 2018). Thus, the primary role(s) for Rqh1 in fission yeast during DSB repair likely involves regulation of strand invasion structures downstream of resection as part of HDR as it does not influence the use of non–HDR pathways like non-homologous end joining (NHEJ; Hope *et al.*, 2006). There is shift toward increased spontaneous DNA damage in *rqh1Δ* cells (Supplemental Figure S3C), although our criteria to exclude short-lived Rad52 foci as described above equally apply in this context.

In cells lacking Rqh1 we observe two distinct repair outcomes for induced DSBs. In one subset of cells we observe unusually rapid repair (example in Figure 4A), while in the other we observe highly persistent DSBs that fail to localize with the donor sequence (example in Figure 4B). Indeed, the overall rate of productive repair within 90 min of initial Rad52-mCherry loading falls from more than 65% in WT cells to ~40% in *rqh1Δ* cells (Figure 4C), suggesting that loss of Rqh1 negatively impacts repair as a whole. However, we also observe that *rqh1Δ* cells that successfully complete repair tend to do so faster than WT cells (Figure 4D). Given Rqh1's role in D-loop disassembly, we next examined whether the more rapid repair reflected a higher likelihood that a strand invasion event leads to repair. Indeed, we observe far fewer encounters between the DSB and donor in *rqh1Δ* cells that successfully repair, both in the population as a whole (Figure 4E) and within individual cells, where we often fail to visualize colocalization before repair within the 5 min frame rate (Figure 4F). This suggests that loss of Rqh1 decreases the number and/or lifetime of homologous strand invasion events, although as demonstrated above for WT cells when imaging at 2 min time points (Supplemental Figure S3, A and B), we may be missing

shorter-lived strand invasion events that contribute to repair. Overall these observations suggest that repair in *rqh1Δ* cells is bimodal, either being more efficient than in WT cells (tending to involve fewer and/or shorter colocalization events) or by failing entirely to complete repair within our experimental observation window.

Conclusion

Taken together, our data indicate a highly efficient homology search and HDR in fission yeast. Surprisingly, we observe not one but multiple site-specific and Rad51-dependent colocalization events between the DSB and donor before many successful repair events. This suggests that 1) the first successful homology search event is not always followed by repair and/or 2) multiple strand invasion events contribute to repair, likely by synthesis dependent strand annealing. Notably, multiple encounters between a DSB and a donor sequence have been proposed previously (Piazza *et al.*, 2017; Piazza and Heyer, 2019) and occur in the context of mating type switching (Houston and Broach, 2006) and meiosis (Ahuja *et al.*, 2021) in budding yeast. The Symington and Heyer groups (Smith *et al.*, 2007; Piazza *et al.*, 2017) also describe evidence for multiple strand invasions in *Saccharomyces cerevisiae* mitotic repair through the use of multiple templates during events leading to translocations, either sequentially by one invasion structure or concurrently through interaction with multiple donors. However, multiple strand invasions are not restricted to repair utilizing homeologous templates or to yeasts; they have also been invoked in *Drosophila*, which relies heavily on SDSA for DSB repair (Adams *et al.*, 2003; McVey *et al.*, 2004).

While we suggest that the observed dissolution of D-loops by Rqh1 likely reflects its contribution to promoting repair by SDSA (Supplemental Figure S4A), it may also facilitate rejection of strand invasion intermediates with nonhomologous or homeologous sequences (Supplemental Figure S4B); the latter could explain why we often observe concomitant repair failure and lack of colocalization events in cells lacking Rqh1. Indeed, expression of mutated forms of Sgs1 (the orthologue of BLM and Rqh1) abrogated colocalization events between a DSB and the repair template in budding yeast (Piazza *et al.*, 2017). A subset of cells displaying rapid repair in the absence of Rqh1 could also reflect sister-chromatid conversion, an HDR outcome that would also make the donor sequence dispensable and that has been shown to be up-regulated in *rqh1Δ* cells (Hope *et al.*, 2006). However, 1) both sister chromatids are likely to be cut simultaneously (Leland *et al.*, 2018) and 2) sister chromatin conversion (SCC) reconstitutes the HO nuclease cut site and therefore would be expected to lead to repeated rounds of DSB induction, which we do not observe. We also acknowledge that we could fail to observe some short-lived encounters in *rqh1Δ* cells due to our observation frequency. More broadly, new insights into the highly transient nature of D-loop processing in budding yeast (Piazza *et al.*, 2019) support the possibility of short-lived encounters that are regulated by Rqh1. We also note that events that cannot be resolved by diffraction-limited live-cell microscopy, such as local strand eviction and reinvasion as well as migration of homology search invasion structures, could take place during colocalization and are likely to be regulated by Rqh1. In patients with mutations in BLM, the numbers of mitotic and meiotic crossover events are greatly increased, leading to genome instability and cancer predisposition, among other symptoms (Arora *et al.*, 2014). Thus, we infer that strand invasion in cells with HO-induced DSBs lacking Rqh1 may be more likely to lead to crossover repair. Our observations suggest that defects in the ability to promote non–crossover repair by SDSA combined with an accumulation of dead-end repair intermediates could contribute to disease etiology, consistent with the observation that mutated
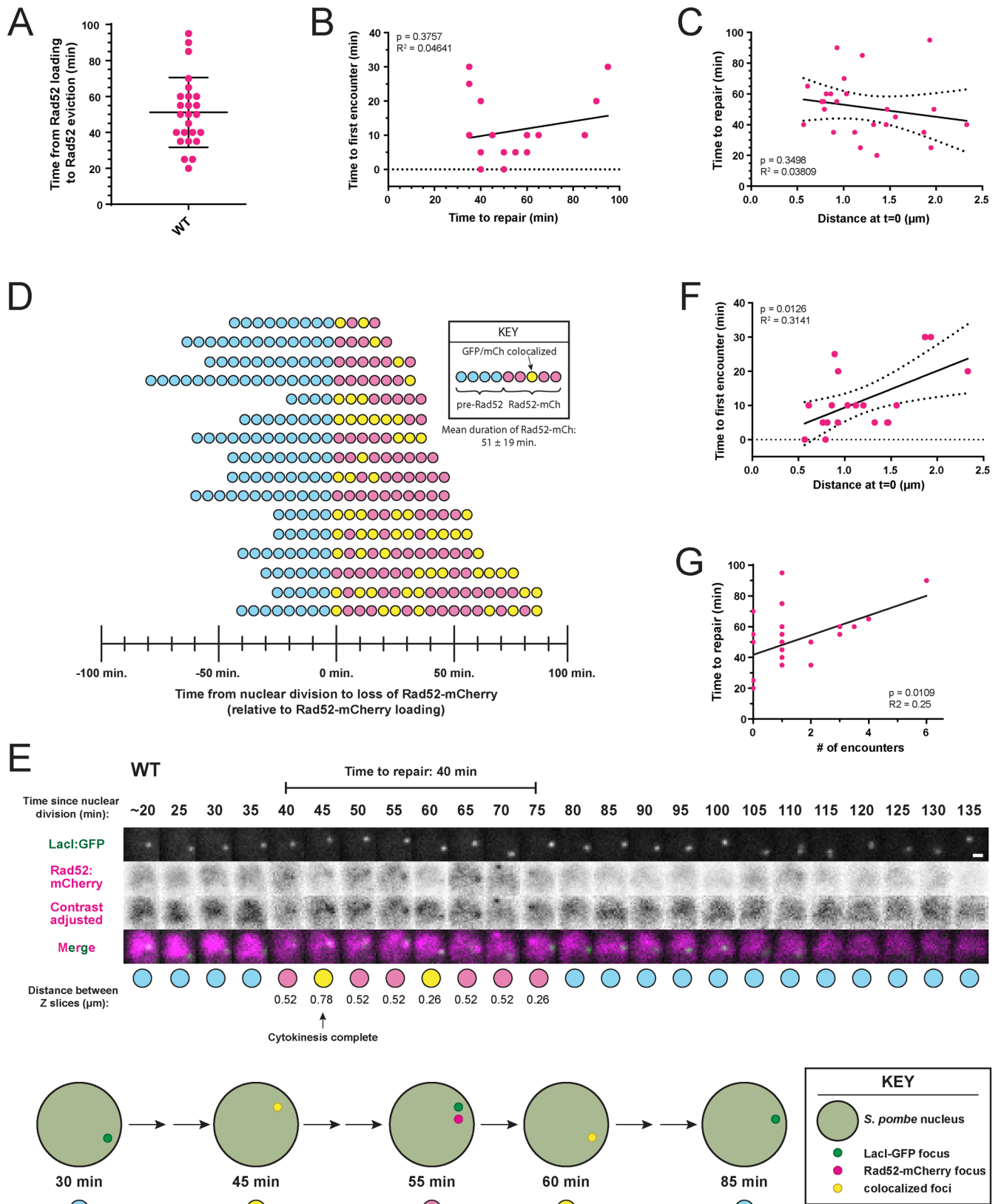
FIGURE 3: HDR in fission yeast frequently involves multiple encounters between the DSB and donor sequence. WT cells were imaged as described in *Materials and Methods*. Data points in A–C, F, and G represent individual cells. (A) Repair of WT fission yeast cells is highly efficient in our induced DSB system. Time to repair was measured as the time in minutes from the first appearance of a site-specific DSB (persistent Rad52-mCherry focus) to its disappearance for at least three consecutive frames (5 min intervals, *n* = 25). Mean = 51.2, SD = 19.4. Plot reflects mean and SD. (B) Timing of the first encounter between the DSB and donor sequence and timing of repair are not correlated. Time to

alleles of Rqh1 lead to the "cut" phenotype in fission yeast treated with DNA-damaging agents (Stewart *et al.*, 1997).

Further study is also needed to fully define the relationship between genome organization and HDR efficiency and outcome. We find that the initial position of the DSB relative to the donor sequence had no bearing on overall repair duration, although DSBs that began closer to the donor sequence realized a first colocalization event more efficiently. Earlier studies of ectopic HDR have documented a correlation of initial position with repair efficiency in budding yeast (Agmon *et al.*, 2013; Lee *et al.*, 2016). However, a lack of correlation is reported in a more recent budding yeast *trans* reporter NHEJ study (Sunder and Wilson, 2019), in line with our results. Of note, DSB induction in a budding yeast mutant with reduced local chromatin mobility suggests that mobility of the remaining global chromatin, including the donor, is crucial for ectopic HDR (Cheblal *et al.*, 2020). While this could reflect inherent differences between model organisms, we also note that these studies leverage a relatively short-range homologous cassette inserted at ectopic sites rather than the homologous chromosome employed here. Beyond a role for mobility, our observations suggest that, although dependent on homology search, repair efficiency in this system is more greatly influenced by the number of strand invasion events. One possibility is that while D-loop dissolution promotes SDSA, it also limits the extent of synthesis from a single homology search event (Supplemental Figure S4, A and B). Thus, multiple strand invasion cycles may be necessary for the extent of synthesis required to span the initial DSB to take place, thereby supporting subsequent strand annealing and repair.

MATERIALS AND METHODS
Request a protocol through *Bio-protocol*.

Yeast culture, strain construction, and DSB induction
The strains used in this study are listed in Supplemental Table S1. *S. pombe* cells were grown, maintained, and crossed using standard procedures and media (Moreno *et al.*, 1991). Gene replacements were made by gene replacement with various MX6-based drug resistance genes (Bähler *et al.*, 1998; Hentges *et al.*, 2005). In one haploid h- strain, the 10.3 kb LacO array was inserted between *Mmf*1 and *Apl*1 on the right arm of Chr II (3,442,981) using a modified two-step integration procedure that first creates a site-specific DSB to increase targeting efficiency of linearized plasmid pSR10_ura4_10.3kb (Rohner *et al.*, 2008; Leland *et al.*, 2018). In another haploid *mat2-102* strain (competent to make a stable diploid when mated with an h- strain), a modified MX6-based hygromycin-resistance cassette containing the HO cut site was inserted between *Apl*1 and *Mug*178 on Chr II (3,446,249). This insertion is 3.2 kb distal to the site of LacO insertion in the h- strain. DSB induction using the Purg1lox-HO system was performed as previously described (Leland and King, 2014; Leland *et al.*, 2018).

DSB induction using Purg1lox-HO
We used the uracil-responsive Purg1lox expression system, with slight modifications, to induce HO endonuclease expression and create site-specific DSBs at the HO cut site (Watt *et al.*, 2008; Watson *et al.*, 2011). We performed a fresh integration of the HO gene at the endogenous *urg1* locus for each experiment in order to reduce long-term instability at the HO cut site or the development of HO resistance, presumably due to insertion/deletion events caused by basal expression levels of HO. The pAW8EN*del*-HO plasmid (a gift from Tony Carr, The University of Sussex) was transformed into *S. pombe* cells, which were then plated onto Edinburgh minimal media (EMM)-leu+thi-ura plates (–leucine: plasmid selection; +thiamine: Pnmt1-Cre repression; –uracil: Purg1lox-HO repression). After 4–6 d of growth at 30°C, 20–60 individual colonies were combined to obtain a reproducible plasmid copy number across the population. Cre-mediated HO gene exchange at the endogenous Urg1 locus (urg1::RMCEkanMX6) was induced by overnight culture in EMM-thi-ura+ade+NPG media (–thiamine: expression of Cre from pAW8ENdel-HO; –uracil: Purg1lox-HO repression; +0.25 mg/ml adenine: reduce autofluorescence; +0.1 mM *n*-propyl gallate [NPG]: reduce photobleaching in microscopy experiments, prepared fresh).

first encounter is the difference between the first frame when Rad52-mCherry is visualized and the first colocalization event. Time to repair was measured as in A. Linear regression: *p* value = 0.3757, $R^2 = 0.04641$ (*n* = 16). (C) Timing of repair and initial distance is not correlated. Initial distance between the DSB and donor sequence was measured as the three-dimensional distance between the centers of the Rad52-mCherry (DSB) and LacI-GFP (donor) foci in the first frame after appearance of a site-specific (persistent) Rad52-mCherry focus. Time to repair was measured as in A. Linear regression: *p* value = 0.3498, $R^2 = 0.03809$ (*n* = 24). Confidence bands reflect the 95% confidence interval. (D, E) Many WT cells with induced DSBs experience multiple colocalization events with the homologous donor sequence during repair, with variability in repair timing as well as number and length of colocalizations. (D) Graph of colocalization events of Rad52-mCherry (DSB) and LacI-GFP (donor) foci in representative WT cells with an induced DSB. Each row represents one individual cell, and each circle represents a time point taken every 5 min. Blue circles: time from nuclear division to Rad52-mCherry loading. Pink circles: time from Rad52-mCherry loading to unloading for at least three consecutive frames. Yellow circles: colocalization of the DSB (Rad52-mCherry) and donor (LacI-GFP bound to *lacO* repeats at *mmf1*) foci. See Supplemental Figure S2 for additional representative cells. (E) Representative cell exhibiting multiple colocalizations during repair of the HO-induced DSB. Time of nuclear division was estimated based on cytokinesis in bright-field images. Images were acquired every 5 min (columns) and are indicated relative to nuclear division (see *Materials and Methods* for details). Contrast of Rad52-mCherry signal adjusted according to the full histogram of intensities where indicated. Scale bar = 1 µm. Bottom, cartoon depicts examples of the key events over the time course: at 10 min, LacI-GFP is present at the donor; at 45 min, there is colocalization of the Rad52-mCherry and LacI-GFP foci; at 55 min, the foci are no longer colocalized; at 60 min, the foci have again colocalized; and at 105 min, Rad52-mCherry is absent from the DSB. (F) Timing of the first encounter between the DSB and donor sequence is correlated with the distance between their initial positions. Time to first encounter is the difference between the first frame when Rad52-mCherry is visualized and the first colocalization event. Initial distance was measured as in C. Linear regression: *p* value = 0.0126, $R^2 = 0.3141$ (*n* = 18). Confidence bands reflect the 95% confidence interval. (G) The number of individual encounters is correlated with the timing of repair in individual cells. # of visualized encounters indicates the number of separate encounters (one or more consecutive frames [at 5 min intervals] with colocalization) between the DSB and donor. Time to repair was measured as in A. Linear regression: *p* value = 0.0109, $R^2 = 0.25$ (*n* = 20).
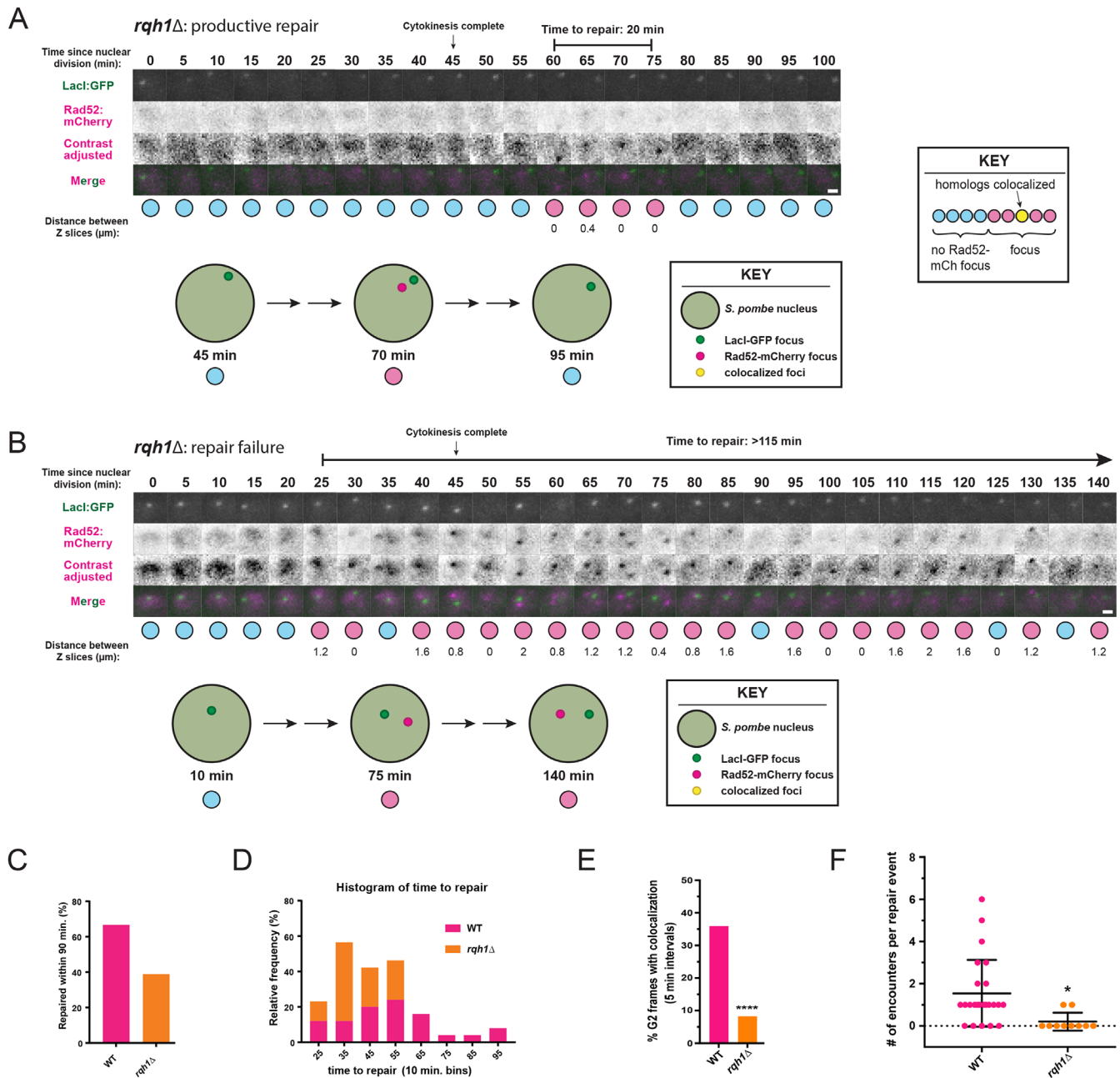
FIGURE 4: Cells lacking Rqh1 display a bimodal repair phenotype and have fewer encounters between the induced DSB and donor during repair. (A) Successful repair events are often relatively short in *rqh1Δ* cells with induced DSBs. Z stack images of a representative *rqh1Δ* cell nucleus showing productive repair of the induced DSB (persistent loss of Rad52-mCherry signal for at least three frames). Imaging as described in *Materials and Methods* with 5 min between each time frame (columns). Contrast of Rad52-mCherry signal adjusted to the full histogram of intensities where indicated. Scale bar = 1 μm. Bottom, cartoon depicts examples of the key events over the time course: at 45 min, LacI-GFP is present at the donor; at 70 min, Rad52-mCherry is loaded at the DSB but not colocalized to the donor; and at 95 min, Rad52-mCherry is absent from the DSB. (B) Failure to repair DSBs efficiently is more prevalent in *rqh1Δ* cells with the induced DSB. Z stack images of a representative *rqh1Δ* cell nucleus showing repair failure (persistence of Rad-52mCherry signal >90 min). Imaging as described in *Materials and Methods* with 5 min between each time frame (columns). Contrast of Rad52-mCherry signal adjusted according to full histogram of intensities where indicated. Scale bar = 1 μm. Bottom, cartoon depicts examples of the key events over the time course: at 10 min, LacI-GFP is present at the donor; at 75 min, Rad52-mCherry is loaded at the DSB; and at 140 min, Rad52-mCherry persists at the DSB without having colocalized with the donor. (C) Cells lacking Rqh1 are less likely to undergo efficient DSB repair than WT cells. Total percentage of WT (*n* = 37) and *rqh1Δ* (*n* = 37) cells with an induced DSB repair within 90 min. (D) Cells lacking Rqh1 that successfully repair the induced DSB do so more rapidly than in WT cells. Stacked (no data hidden) relative frequency histograms of time to repair (10 min bins) in WT cells (pink, *n* = 21; see Figure 3A) and *rqh1Δ* cells (orange, *n* = 16) with the induced DSB. (E) Cells lacking Rqh1 have a significantly smaller proportion of G2 frames with a colocalization between the induced DSB and donor sequence per cell compared with WT. Quantification of

colocalization of DSB (Rad52-mCherry) and donor sequence (LacI-GFP bound to *lacO* repeats at *mmf1*). Frames in which cells were in G2 phase were analyzed for colocalization of DSB and donor and assembled as a total percentage across all cells. ****$p < 0.0001$, Kolmogorov–Smirnov test of cumulative distributions (of percentages from individual cells). WT: $n = 26$, *rqh1Δ*: $n = 37$. WT data replotted from Figure 2C. (F) Cells lacking Rqh1 have significantly fewer encounters between the DSB and donor per repair event relative to WT cells. # of encounters per repair indicates the number of separate encounters (one or more consecutive frames at 5 min intervals with colocalization) between the DSB and donor in individual WT ($n = 25$) or *rqh1Δ* ($n = 10$) cells. *$p = 0.0143$, Kolmogorov–Smirnov test of cumulative distributions. Plot reflects mean and SD.

The following day, site-specific DSBs were induced in log-phase cultures by the addition of 0.50 mg/ml uracil. This induction strategy resulted in ~15% of cells making a DSB within ~2 h (Supplemental Figure S1A).

Microscopy

All images were acquired on a DeltaVision wide-field microscope (Applied Precision/GE) using a 1.2 NA 100× objective (Olympus), solid-state illumination, and an Evolve 512 EMCCD camera (Photometrics). Slides were prepared ~10–20 min after adding 0.50 mg/ml uracil to log-phase cultures to induce HO endonuclease expression and DSB formation. Cells were mounted on 1.2% agar pads (EMM +0.50 mg/ml uracil, +2.5 mg/ml adenine, +0.1 mM freshly prepared NPG) and sealed with VALAP (1:1:1 vaseline:lanolin:paraffin). Image acquisition began between 40 and 80 min after uracil addition. Imaging parameters for all microscopy assay data acquisition were as follows. Transmitted light: 35% transmittance, 0.015 s exposure; mCherry: 32% power, 0.08 s exposure; GFP: 10% power, 0.05 s exposure. At each time point (every 5 min for 2.5–4 h), 25 Z-sections were acquired at 0.26 mm spacing (16 Z-sections were acquired at 0.42 mm spacing to mitigate photobleaching in some samples).

Image analysis

For the microscopy assay of interhomologue repair, data were acquired for each cell cycle individually, including time of nuclear division, time of cytokinesis, frames in which Rad52-mCherry focus was visible, and frames in which Rad52-mCherry focus colocalized with the LacI-GFP focus at the diffraction limit (in the case of the 2 *lacO* at *mmf1* strain [Figure 2, A and B], colocalizations between both LacI-GFP foci were recorded instead). Time to repair was measured as the time in minutes from the first appearance of a site-specific DSB (persistent rad52-mCherry focus) to its disappearance for at least three consecutive frames. Only site-specific DSBs (defined as Rad52-mCherry focus persistence for at least four frames that began in late S- or early G2-phase) were considered, because spontaneous DSB events can occur within the genome especially in G1- and early S-phase (see Supplemental Figure 1, B and C). Fields were analyzed manually, using the same contrast settings for mCherry and GFP channels for consistency. Images from representative cells for each strain (Figures 1C, 2, B and D, 3E, and 4, A and B, and Supplemental Figures S1D and S2, A–C) were prepared using ImageJ macros to automate merge and montage image creation using the same gate size (height and width), while allowing for manual selection of the Z plane and centering on the nucleus. For visual clarity, the contrast of some images was adjusted according to the histogram using Levels sampling functions of Adobe Photoshop (2018) to set the darkest pixel as black and the brightest pixel as white. Merged images are either max projection or single planes with Rad52-mCherry in focus for visual clarity. The distance between Z slices for each frame is the distance in Z between the Z slice containing the center of the LacI-GFP focus and the Z slice containing the center of the Rad52-mCherry focus (or the center of the nucleus [denoted by the middle Z slice of diffuse Rad52-mCherry signal] in frames with no Rad52-mCherry focus).

Data were plotted and analyzed using GraphPad Prism 7.01. Percentages of G2 frames with colocalization from individual cells were analyzed using the Kolmogorov–Smirnov test of cumulative distributions (Figures 2C and 4E; p value denoted by asterisks and average plotted), relative frequency histograms (Figure 2E), and cumulative frequency histograms (Figure 2F). Linear regressions (Figure 3, B and -C, and E and F) were calculated using default Prism settings. Dotted lines (Figure 3, C and F) represent 95% confidence intervals. The numbers of encounters per repair (Figure 4F) were analyzed using the Kolmogorov–Smirnov test of cumulative distributions (mean and SD plotted).

Marker loss assay

To examine repair outcome of the DSB in our system results based on sequence changes resulting from different repair pathways at the HO cut site, we performed a marker loss assay to assess the proportion of induced cells in which the MX6-based drug resistance gene (Bähler *et al.*, 1998; Hentges *et al.*, 2005) was lost due to use of the donor sequence during HDR. DSB induction was performed on WT diploid *S. pombe* cells as described above. At 2 h following induction in log phase (growth for 2 h in EMM-ura+ade+NPG with uracil added), cells were resuspended in EMM-ura media and plated to yeast extract with 5 supplements media (YE5S) at 1:1000 ($n = 3$), 1:2000 ($n = 3$), and 1:5000 ($n = 2$) dilutions. After 24 h, YE5S plates were replica plated to YE5S+kanamycin (at HO cut site—lost when the DSB is repaired using the homologous donor) and YE5S+hygromycin (at *urg1*::RMCE—lost when the pAW8E*Nde*l-HO plasmid is flipped in via Cre recombination before induction). Colonies were counted with a Bio-Rad Molecular Imager VersaDoc (total colony count between 50 and ~160 cells per YE5S plate). The percentage of cells from each YE5S plate that had repaired by interhomologue HDR was calculated as (%Kan sensitive colonies/%Hyg sensitive colonies)*100. Data along with mean and SD were plotted using GraphPad Prism 7.01.

REFERENCES

Adams MD, McVey M, Sekelsky JJ (2003). Drosophila BLM in double-strand break repair by synthesis-dependent strand annealing. Science 299, 265–267.

Agmon N, Liefshitz B, Zimmer C, Fabre E, Kupiec M (2013). Effect of nuclear architecture on the efficiency of double-strand break repair. Nat Cell Biol 15, 694–699.

Ahuja JS, Harvey CS, Wheeler DL, Lichten M (2021). Repeated strand invasion and extensive branch migration are hallmarks of meiotic recombination. Mol Cell 81, 4258–4270.e4.

Arora H, Chacon AH, Choudhary S, McLeod MP, Meshkov L, Nouri K, Izakovic J (2014). Bloom syndrome. Int J Dermatol 53, 798–802.

Bachrati CZ, Borts RH, Hickson ID (2006). Mobile D-loops are a preferred substrate for the Bloom's syndrome helicase. Nucleic Acids Res 34, 2269–2279.

Bähler J, Wu JQ, Longtine MS, Shah NG, McKenzie A 3rd, Steever AB, Wach A, Philippsen P, Pringle JR (1998). Heterologous modules for efficient and versatile PCR-based gene targeting in Schizosaccharomyces pombe. Yeast 14, 943–951.

Bodi Z, Gysler-Junker A, Kohli J (1991). A quantitative assay to measure chromosome stability in Schizosaccharomyces pombe. Mol Gen Genet 229, 77–80.

Bonilla CY, Melo JA, Toczyski DP (2008). Colocalization of sensors is sufficient to activate the DNA damage checkpoint in the absence of damage. Mol Cell 30, 267–276.

Cheblal A, Challa K, Seeber A, Shimada K, Yoshida H, Ferreira HC, Amitai A, Gasser SM (2020). DNA damage-induced nucleosome depletion enhances homology search independently of local break movement. Mol Cell 80, 311–326.e4.

Coulon S, Noguchi E, Noguchi C, Du LL, Nakamura TM, Russell P (2006). Rad22Rad52-dependent repair of ribosomal DNA repeats cleaved by Slx1-Slx4 endonuclease. Mol Biol Cell 17, 2081–2090.

Egel R (1973). Genes involved in mating type expression of fission yeast. Mol Gen Genet 122, 339–343.

Haber JE (1998). Mating-type gene switching in Saccharomyces cerevisiae. Annu Rev Genet 32, 561–599.

Haber JE (2018). DNA Repair: the search for homology. Bioessays 40, e1700229.

Hentges P, Van Driessche B, Tafforeau L, Vandenhaute J, Carr AM (2005). Three novel antibiotic marker cassettes for gene disruption and marker switching in Schizosaccharomyces pombe. Yeast 22, 1013–1019.

Hope JC, Cruzata LD, Duvshani A, Mitsumoto J, Maftahi M, Freyer GA (2007). Mus81-Eme1-dependent and -independent crossovers form in mitotic cells during double-strand break repair in Schizosaccharomyces pombe. Mol Cell Biol 27, 3828–3838.

Hope JC, Mense SM, Jalakas M, Mitsumoto J, Freyer GA (2006). Rqh1 blocks recombination between sister chromatids during double strand break repair, independent of its helicase activity. Proc Natl Acad Sci USA 103, 5875–5880.

Houston PL, Broach JR (2006). The dynamics of homologous pairing during mating type interconversion in budding yeast. PLoS Genet 2, e98.

Laurenson P, Rine J (1992). Silencers, silencing, and heritable transcriptional states. Microbiol Rev 56, 543–560.

Lee C-S, Wang RW, Chang H-H, Capurso D, Segal MR, Haber JE (2016). Chromosome position determines the success of double-strand break repair. Proc Natl Acad Sci USA 113, E146–E154.

Leland BA, Chen AC, Zhao AY, Wharton RC, King MC (2018). Rev7 and 53BP1/Crb2 prevent RecQ helicase-dependent hyper-resection of DNA double-strand breaks. eLife 7, e33402.

Leland BA, King MC (2014). Using LacO arrays to monitor DNA double-strand break dynamics in live Schizosaccharomyces pombe cells. Methods Mol Biol 1176, 127–141.

Lorenz A, Mehats A, Osman F, Whitby MC (2014). Rad51/Dmc1 paralogs and mediators oppose DNA helicases to limit hybrid DNA formation and promote crossovers during meiotic recombination. Nucleic Acids Res 42, 13723–13735.

Lorenz A, Osman F, Folkyte V, Sofueva S, Whitby MC (2009). Fbh1 limits Rad51-dependent recombination at blocked replication forks. Mol Cell Biol 29, 4742–4756.

McVey M, Adams M, Staeva-Vieira E, Sekelsky JJ (2004). Evidence for multiple cycles of strand invasion during repair of double-strand gaps in Drosophila. Genetics 167, 699–705.

Mehta A, Haber JE (2014). Sources of DNA double-strand breaks and models of recombinational DNA repair. Cold Spring Harb Perspect Biol 6, a016428.

Mimitou EP, Symington LS (2009). Nucleases and helicases take center stage in homologous recombination. Trends Biochem Sci 34, 264–272.

Miné-Hattab J, Recamier V, Izeddin I, Rothstein R, Darzacq X (2017). Multi-scale tracking reveals scale-dependent chromatin dynamics after DNA damage. Mol Biol Cell 28, 3323–3332.

Miné-Hattab J, Rothstein R (2012). Increased chromosome mobility facilitates homology search during recombination. Nat Cell Biol 14, 510–517.

Moreno S, Klar A, Nurse P (1991). Molecular genetic analysis of fission yeast Schizosaccharomyces pombe. Methods Enzymol 194, 795–823.

Nanbu T, Nguyễn LC, Habib AG, Hirata N, Ukimori S, Tanaka D, Masuda K, Takahashi K, Yukawa M, Tsuchiya E, et al. (2015). Fission yeast Exo1 and Rqh1-Dna2 redundantly contribute to resection of uncapped telomeres. PLoS One 10, e0140456.

Ohle C, Tesorero R, Schermann G, Dobrev N, Sinning I, Fischer T (2016). Transient RNA-DNA hybrids are required for efficient double-strand break repair. Cell 167, 1001–1013.e7.

Pâques F, Haber JE (1999). Multiple pathways of recombination induced by double-strand breaks in Saccharomyces cerevisiae. Microbiol Mol Biol Rev 63, 349–404.

Piazza A, Heyer WD (2019). Moving forward one step back at a time: reversibility during homologous recombination. Curr Genet 65, 1333–1340.

Piazza A, Shah SS, Wright WD, Gore SK, Koszul R, Heyer WD (2019). Dynamic processing of displacement loops during recombinational DNA repair. Mol Cell 73, 1255–1266.e4.

Piazza A, Wright WD, Heyer WD (2017). Multi-invasions are recombination byproducts that induce chromosomal rearrangements. Cell 170, 760–773.e15.

Renkawitz J, Lademann CA, Jentsch S (2014). Mechanisms and principles of homology search during recombination. Nat Rev Mol Cell Biol 15, 369–383.

Rohner S, Gasser SM, Meister P (2008). Modules for cloning-free chromatin tagging in Saccharomyces cerevisae. Yeast 25, 235–239.

Saad H, Gallardo F, Dalvai M, Tanguy-le-Gac N, Lane D, Bystricky K (2014). DNA dynamics during early double-strand break processing revealed by non-intrusive imaging of living cells. PLoS Genet 10, e1004187.

Sanchez A, Sharma S, Rozenzhak S, Roguev A, Krogan NJ, Chabes A, Russell P (2012). Replication fork collapse and genome instability in a deoxycytidylate deaminase mutant. Mol Cell Biol 32, 4445–4454.

San Filippo J, Sung P, Klein H (2008). Mechanism of eukaryotic homologous recombination. Annu Rev Biochem 77, 229–257.

Schonbrun M, Kolesnikov M, Kupiec M, Weisman R (2013). TORC2 is required to maintain genome stability during S phase in fission yeast. J Biol Chem 288, 19649–19660.

Seeber A, Dion V, Gasser SM (2013). Checkpoint kinases and the INO80 nucleosome remodeling complex enhance global chromatin mobility in response to DNA damage. Genes Dev 27, 1999–2008.

Seeber A, Hegnauer AM, Hustedt N, Deshpande I, Poli J, Eglinger J, Pasero P, Gut H, Shinohara M, Hopfner KP, et al. (2016). RPA mediates recruitment of MRX to forks and double-strand breaks to hold sister chromatids together. Mol Cell 64, 951–966.

Smith CE, Llorente B, Symington LS (2007). Template switching during break-induced replication. Nature 447, 102–105.

Stewart E, Chapman CR, Al-Khodairy F, Carr AM, Enoch T (1997). rqh1+, a fission yeast gene related to the Bloom's and Werner's syndrome genes, is required for reversible S phase arrest. EMBO J 16, 2682–2692.

Sunder S, Wilson TE (2019). Frequency of DNA end joining in trans is not determined by the predamage spatial proximity of double-strand breaks in yeast. Proc Natl Acad Sci USA 116, 9481–9490.

Symington LS (2016). Mechanism and regulation of DNA end resection in eukaryotes. Crit Rev Biochem Mol Biol 51, 195–212.

Symington LS, Rothstein R, Lisby M (2014). Mechanisms and regulation of mitotic recombination in Saccharomyces cerevisiae. Genetics 198, 795–835.

van Brabant AJ, Ye T, Sanz M, German JL III, Ellis NA, Holloman WK (2000). Binding and melting of D-loops by the Bloom syndrome helicase. Biochemistry 39, 14617–14625.

Watson AT, Werler P, Carr AM (2011). Regulation of gene expression at the fission yeast Schizosaccharomyces pombe urg1 locus. Gene 484, 75–85.

Watt S, Mata J, López-Maury L, Marguerat S, Burns G, Bähler J (2008). urg1: a uracil-regulatable promoter system for fission yeast with short induction and repression times. PLoS One 3, e1428.

Yan Z, Xue C, Kumar S, Crickard JB, Yu Y, Wang W, Pham N, Li Y, Niu H, Sung P, et al. (2019). Rad52 restrains resection at DNA double-strand break ends in yeast. Mol Cell 76, 699–711.e6.

Zimmer C, Fabre E (2019). Chromatin mobility upon DNA damage: state of the art and remaining questions. Curr Genet 65, 1–9.